Two types of antigorite serpentinite controlling heterogeneous slow-slip behaviours of slab-mantle interface

メタデータ	言語: eng
	出版者:
	公開日: 2017-10-03
	キーワード (Ja):
	キーワード (En):
	作成者:
	メールアドレス:
	所属:
URL	https://doi.org/10.24517/00010739

Title:

Two types of antigorite serpentinite controlling heterogeneous slow-slip behaviours of slab-mantle interface

Authors:

Tomoyuki Mizukami[1], Hironori Yokoyama[1], Yoshihiro Hiramatsu[1], Shoji Arai[1], Hirokazu Kawahara[2], Takayoshi Nagaya[2] and Simon R. Wallis[2]

Affiliations:

1. Department of Earth Sciences, Graduate School of Environmental Studies, Kanazawa University, Kanazawa 920-1192, Japan.

2. Department of Earth and Planetary Sciences, Graduate School of Environmental Studies, Nagoya University, Nagoya 606-8601, Japan

Corresponding author: Tomoyuki Mizukami

e-mail address: peridot@staff.kanazawa-u.ac.jp

tel: +81-76-264-6509

fax: +81-76-264-6513

ABSTRACT

It is known that plate boundaries in subduction zones show heterogeneous slip nature with strongly coupled seismogenic zones and various types of episodic tremor and slip (ETS) zones. In order to examine the petrological controls on the large-scale structure, we compared recent geophysical observations in the Shikoku area, southwest Japan with petrological models of the hanging wall mantle wedge. As a result, we found a close relationship between mineral assemblages in the mantle wedge and the characteristics of slow slip behaviour recorded in the Shikoku area: Short-term ETSs take place in the antigorite + olivine stability field and silent long-term slow slip events (SSEs) take place in the antigorite + brucite stability field. Based on observations of natural antigorite serpentinites, we propose a model that the dominant serpentinization reaction in the mantle wedge changes with increasing depth resulting in variable extents of pore fluid pressures along slip planes. The serpentinization reaction in the antigorite + brucite stability field (olivine + H_2O $\rightarrow$ antigorite + brucite) proceeds at the expense of water. This is consistent with moderately elevated pore pressures inferred for long-term SSEs. The existence of weak brucite enhances the development of shear zones oblique to the main foliation. The resultant anastomosing network provides fluid pathways that may help reduce pore pressures on slip planes. In contrast, progress of the serpentinization reaction in the antigorite + olivine stability field (olivine + H_2O + SiO_2 $\rightarrow$ antigorite) results in a large amount of residual water that contributes to further increase pore fluid pressures on slip planes of short-term SSEs. Our results imply that understanding of serpentinization reactions and their contributions to fluid networks in mantle wedge is important in constructing quantitative 3-D models for strain evolutions along plate boundaries.

Keywords Slow slip events, pore fluid pressure, serpentinite, antigorite, brucite

1. Introduction

Plate boundaries in convergent settings form major thrust faults that periodically induce great earthquakes with magnitudes greater 8 (Ando, 1975; Schwartz and Rokosky, 2007). Quantitative understanding of the seismogenic system is one of the most important goals in earth science, and an important motivation for carrying out geological studies of the development of large-scale structures in ancient subduction complexes as well as many geophysical studies of present-day subduction processes and related structures, including laboratory work on rock physics and geophysical modelling.

The deployment of a dense network of geodetic and seismic observations has revealed the existence of 'silent' phases of episodic tremor and slip (ETS) in the downdip portions of seismogenic zones (Dragert *et al.*, 2001; Obara, 2002; Rogers and Dragert, 2003). ETS relieves significant amounts of shear stress during inter-seismic intervals (Hirose and Obara, 2006; Hiramatsu *et al.*, 2008; Hirose *et al.*, 2010) and it is considered to play a significant role in localizing elastic strain in the neighbouring updip seismogenic zone that eventually leads to the formation of a large earthquake (Matsuzawa *et al.*, 2010). An increasing body of geophysical observations confirm that this type of heterogeneous slip consists of strongly coupled seismogenic zones at shallow levels that lead into ductilely deforming non-seismic domains separated by ETS domains of various sizes and that this division is a fundamental characteristic of subduction zone plate boundaries (Obara and Hirose, 2006; Obara, 2010; 2011). One of the key pieces of information that is lacking is a better understanding of the geological controls on the large-scale frictional heterogeneity.

Several characteristics of ETS suggest low effective normal stresses on the slip planes (Shelly *et al.*, 2006; Schwartz and Rokosky, 2007; Ide, 2010; Obara, 2011). For example, tremor activities take place in short intervals and are often triggered by small changes of local stress (several hundred Pa) due to seismic surface waves and tides (Rubinstein *et*

al., 2007; 2008). Only minor stress changes are observed during slow slip events (SSEs) (Ozawa *et al.*, 2002; Schmidt and Gao, 2010). The association of ETS with domains of low effective stress is generally explained by the presence of high pore-fluid pressures and this is supported by the high Poisson's ratios observed in the domains where ETS occurs (Kodaira *et al.*, 2004; Shelly *et al.*, 2007; Matsubara *et al.*, 2009; Schmidt and Gao, 2010). Katayama *et al.* (2012) demonstrated that foliated antigorite-rich serpentinite can constrain slab-derived fluid to move along the slab-mantle interface resulting in high pore pressure at the tip of the mantle wedge, the most dominant ETS locality. However, this model does not explain heterogeneous distributions of domains of SSEs. This heterogeneity is probably due to spatial variations in effective normal stress, physical properties of the rock, or geometry of the subduction plate interface. Peacock (2009) examined dehydration reactions in oceanic slab as a cause of high pore pressure based on numerical calculations of subduction zone thermal structures. However, the calculated depths for fluid release are not coincident with the observed ETS localities.

In this contribution, we propose that depending on the thermal structure two different types of antigorite serpentinite with different mineral assemblages can develop in hanging wall mantle. We then examine the relationship between the metamorphic transition between these two types of serpentinite and the observed depth-dependent transition in slip behaviour observed in western Shikoku in the Nankai subduction zone, which is one the best characterized zones of ETS in the world.

2. Two types of antigorite serpentinite

Mineral assemblages in hydrated mantle depend on the bulk rock composition and the chemistry of the hydrating fluid as well as temperature and pressure conditions. Appropriate bulk rock compositions of the mantle wedge that becomes serpentinized can be inferred from peridotite xenoliths in arc magmas (Arai and Ishimaru, 2008) and forearc peridotite exposed at trench slopes (Parkinson and Pearce, 1998). Extensive

partial melting of mantle wedge in wet conditions results in a mantle consisting dominantly of harzburgite and dunite with olivine (Ol) making up more that >70 vol% and smaller amounts of orthopyroxene (Opx). We can assume this type of lithology with low contents of Ca, Al and incompatible elements and with a high Mg/Fe ratio dominates the mantle wedge of southwest Japan because extremely high degrees of mantle melting have caused extensive volcanic activities of high-Mg andesite (HMA) at the earliest stage of the PSP subduction in middle Miocene (Tatsumi, 2006). Olivine-rich lithology is also formed at the base of the arc crust through crystal settling from olivine-saturated magmas including the HMA. Results of seismic experiments show the existence of a high velocity layer with internal reflections indicating a layered structure (Ito *et al.*, 2009). Petrological evidence for olivine + pyroxene cumulates is widely found in ultramafic xenoliths in southwest Japan (Arai *et al.*, 2000).

The general ideal formula for antigorite can be given as $Mg_{3m-3}Si_{2m}O_{5m}(OH)_{4m-6}$ (Mellini *et al.*, 1987). However, natural antigorite may also contain significant amounts of Al and Fe. Experimental results show that Al contents in antigorite significantly affect the antigorite-out reaction at high-pressure conditions: antigorite $\rightarrow$ olivine + Opx + H_2O (Ulmer and Trommsdorff, 1995; Wunder and Schreyer, 1997; Bromiley and Pawley, 2003; Padrón-Navarta *et al.*, 2010). Incorporation of Al in antigorite extends its thermal stability by up to 80 ºC. However, the effect of Al decreases with decreasing pressure (Bromiley and Pawley, 2003) and it is inferred to be about half the maximum at depths around continental Moho. The effects of Fe on the same reaction have been examined using thermodynamic calculations (Ulmer and Trommsdorff, 1999; Padrón-Navarta *et al.*, 2010). In practice, only minor effects are expected for the shallowest part of the mantle wedge because extensive partial melting will form a mantle material highly depleted in both Al and Fe (Arai, 1994; Hellebrand *et al.*, 2001). For example, the Al_2O_3 content of peridotite from the Izu-Bonin-Mariana Forearc is consistently less than 1 wt% (Perkinson and Pearce, 1998). The effect on the temperature stability of antigorite is then expected to be about 10 ºC (Padrón-Navarta *et al.*, 2013). In view of the above discussion, we consider that serpentinization of shallow mantle wedge can be approximately discussed in the system MgO-SiO_2-H_2O (MSH).

Phase diagrams for the MSH system (Evans *et al.*, 1976; Ulmer and Trommsdorff, 1999; Bromiley and Pawley, 2003; Evans, 2004) indicate that the stable mineral assemblage in serpentinized harzburgite changes with increasing temperature in the following order: (1) lizardite + brucite (Liz + Brc), (2) antigorite + brucite (Atg + Brc), (3) antigorite + olivine (Atg + Ol). It has been suggested that the Atg + Brc assemblage may be dominant in mantle rocks adjacent to subduction boundaries (Peacock and Hyndman, 1999; Hyndman and Peacock, 2003). However, brucite has not been widely reported in natural antigorite-rich serpentinite. The reasons for the paucity of brucite include breakdown during prograde metamorphism, hindered formation due to high SiO_2 activities in metamorphic fluids and/or relatively high Opx/Ol ratios in initial peridotites (O'Hanley, 1996), conversion to carbonate minerals in near surface environments (Hostetler *et al.*, 1966) and difficulty in identifying fine-grained brucite (Hostetler *et al.*, 1966; Hyndman and Peacock, 2003).

In order to understand the nature of two types of antigorite serpentinite, we present here field and microstructural observations of natural examples from the Sanbagawa metamorphic belt, southwest Japan (Fig. 1), with particular focus on the occurrence of brucite. We present data from two ultramafic units located in the highest metamorphic grade region (the Higashi-akaishi body) and in a medium-grade metamorphic region (the Shiraga body）. Both are considered to be slivers of a paleo mantle wedge that have become incorporated in a subduction complex that formed along the Cretaceous Eurasian margin (Mizukami and Wallis, 2005; Hattori *et al.*, 2010; Endo, 2010; Aoya *et al.*, 2013b). Both originally consisted mainly of dunite with minor or subordinate amounts of pyroxene-bearing lithologies. Figures 1, 2 and 3 show the occurrence of the antigorite serpentinite developed in these ultramafic units. The P-T paths for these units are shown in Figure 4 (Enami *et al.*, 1994; Enami *et al.*, 2004; Mizukami and Wallis, 2005).

The Higashi-akaishi (HA) ultramafic body presents a case of retrograde serpentinization (Fig. 4). The body includes peridotite with a mineral assemblage of garnet lherzolite

that records the maximum pressure condition above 3 GPa (Enami *et al.*, 2004). The exhumation path traces an anticlockwise curve largely within the Atg + Ol stability field that terminates at around 1 GPa (representing the conditions near the continental Moho) (Mizukami and Wallis, 2005). The temperature at the end of this part of the exhumation path is close to the boundary between the Atg + Ol stability and Atg + Brc stability (Fig. 4).

Antigorite serpentinite is dominant in the marginal part of the HA unit (Fig. 1(b)) and the amount of antigorite increases towards the boundary. There has not been a detailed geochemical examination of the fluid-rock interaction that formed this boundary layer, but the underlying subducted crustal units preserve records of a high-pressure evolution that is partly coincident with those of the HA ultramafic body (Mizukami and Wallis, 2005; Mouri and Enami, 2008; Kouketsu *et al.*, 2010) suggesting a relatively simple evolution where the ultramafic unit has reacted with fluids liberated from material of the subducted slab.

The antigorite serpentinite of the HA body is characterized by the presence of a prominent layering reflecting variable degrees of serpentinization (Fig. 2(a)). The proportion of antigorite shows a bi-modal frequency distribution with peaks at 10 vol% and 50 vol% implying a localized hydration reaction driven by a focused fluid flow. In less serpentinized layers, antigorite forms discrete (isolated) grains nucleated along olivine grain boundaries and locally penetrating into olivine (Fig. 2(c)). As the amount of antigorite increases, stacking of the platy crystals becomes dominant (Fig. 2(d)). Such bundle-like antigorite locally encloses discrete grains of antigorite, indicating that the dominant structure has changed from a homogenous tectonic fabric with disseminated antigorite grains to a spaced foliation during the progressive serpentinization.

Sheared structures defined by the alignment of platy antigorite are characteristically seen in the antigorite-rich layers (Fig. 2(b) and (d)). Our micro-Raman analyses identified sub-micron films of brucite between the platy grains of antigorite in shear

zones (Fig. 2(e) and (f)). Considering the P-T path of the HA body (Fig. 3) and small proportion of brucite to antigorite, brucite is interpreted as a retrograde product infiltrated during the exhumation of the Sanbagawa belt. The close association between brucite and such sheared zones is widely observed in the body (Fig. 1(b)). The wide distribution also suggests that SiO_2 activities were relatively low at distances of only a few tens of meters away from quartz-rich meta-sedimentary rocks.

The Shiraga (SG) body is located in the medium grade zone of the Sanbagawa belt (Fig.1(c)). It records prograde metamorphism with peak conditions of 0.7-0.9 GPa and 430-520 ℃ (Enami *et al.*, 1994) (Fig. 4). The P-T conditions overlap the univariant curve of the net-transfer reaction that limits the Atg + Brc assemblage. The protolith is mainly dunite, which has been converted to antigorite serpentinite with lesser amounts of olivine. Olivine occurs as fine prismatic, dendritic or porphyroblastic crystals with high Mg/Fe values and low NiO contents. These petrological features of olivine suggest a metamorphic origin from the reaction between antigorite and brucite (Kunugiza, 1980; 1984) and microstructural evidence for the reaction is commonly seen throughout the body (Fig. 1(c)).

Brucite is distributed throughout the SG body and in the adjacent small ultramafic blocks (Fig. 1(c)) both as prograde and retrograde products. Brucite is closely associated with sheared structures (Fig. 3). Blocks within sheared serpentinite preserve prograde fabrics characterized by equidimensional microstructures, in which antigorite commonly shows complex intergrowth. A mesh-like texture with a core of antigorite rimmed by metamorphic olivine is locally seen (Fig. 3(b)). This texture is very similar to the hourglass texture in antigorite serpentinite from Knee Lake, Manitoba (Wicks *et al.*, 1977). In the sheared matrix, the parallel alignment of antigorite defines a foliation associated with asymmetric S-C structures (Fig. 3 (c), (d) and (e)). It is noted that brucite is concentrated to form thin films sub-parallel to antigorite foliation (Fig. 3). Magnetite after brucite also forms thin veins along shear planes. Conversion of brucite to antigorite and magnetite (due to silica metasomatism) (Fig. 3 (c)) and the presence of undulose extinction in brucite (Fig. 3 (e)) indicate that brucite is present during

deformation and, therefore, that it played a significant role in the development of the sheared structures.

Primary olivine is only rarely observed in the SG body (Kunugiza, 1980) and using the presence of metamorphic olivine as an indicator of a brucite precursor, it can be deduced that the SG body experienced a phase of almost complete serpentinization forming the dominant assemblage Atg + Brc. In contrast, serpentinization of the HA body is much less extensive and limited to the 300 m-thick marginal zone (Fig. 1(b)) after a long evolution in the subduction system (Mizukami and Wallis, 2005). Other ultramafic bodies in the medium grade part of the Sanbagawa belt are reported to be highly serpentinized like the Shiraga body (Kunugiza, 1984). The observations in the Sanbagawa belt suggest that the modal amounts of antigorite in the Atg + Ol serpentinite (e.g. HA body) are significantly less than those in Atg + Brc serpentinite (e.g. SG body).

3. Slow slip events and seismic structures in southwest Japan

In southwest Japan (Fig. 5), the boundary between the Eurasian continental plate and subducting Philippine Sea plate (PSP) is a gently north-dipping thrust boundary with historical records of large earthquakes (Kanamori, 1972; Ando, 1975). Recent results from work using a dense network of observation stations have helped reveal an unprecedented level of detail of the sub-surface structures (Kodaira *et al.*, 2004; Shiomi *et al.*, 2008; Matsubara et al., 2009; Ueno *et al.*, 2008) and active processes along this plate interface (Obara, 2002; Ozawa et al., 2002; Hirose and Obara, 2006; Obara and Hirose, 2006; Hiramatsu *et al.*, 2008; Hirose *et al.*, 2010; Sekine *et al.*, 2010). As a result, it has been established that the low-frequency tremors (typically 2-8 Hz) are widely distributed on the SW Japan subduction boundary at depths of 25-40 km and that their activities temporally coincide with SSEs with active periods of several days (short-term SSEs) (Obara and Hirose, 2006; Shelly *et al.*, 2006; Ide, 2010). Long-term geodetic monitoring has also revealed intermittent activities of more prolonged SSEs

(over several months up to 5 years), referred to as long-term SSEs (Ozawa *et al.*, 2002; Hirose and Obara, 2006).

These two types of SSEs also show distinct distributions. The short-term SSE distributions generally occur at a particular depth and spread laterally affecting a large area. In contrast, long-term SSEs are limited to the Tokai and Bungo Channel areas that define the eastern and western edges of the source areas of the Nankai and the Tonankai earthquakes, respectively (Hirose and Obara, 2006; Sekine *et al.*, 2010) (Fig. 5(a)). The main slip zones of the long-term SSEs are inferred to lie within the subduction boundary at intermediate depths between the seismogenic zone and the short-term ETS sources (Ozawa *et al.*, 2002; Hirose and Obara, 2006).

Recent observations on seismological structures and ETS localities beneath western Shikoku are summarized in Figure 5. The locations of the continental Moho and subducting plate surface are based on receiver function results (Shiomi *et al.*, 2008; Ueno *et al.*, 2008). Seismic tomography shows that low-frequency tremors take place adjacent to a region characterized by high V_P/V_S in the mantle wedge (Matsubara *et al.*, 2009). Projection of the SSE localities (Hirose and Obara, 2006; Sekine *et al.*, 2010) onto selected cross sections (Figure 5(c)) shows that the long-term and short-term SSE localities also coincide with the high V_P/V_S region. High values of V_P/V_S (larger than 1.8) in the mantle are likely explained by the existence of hydrous silicates such as serpentine or an aqueous fluid (Christensen, 2004; Matsubara *et al.*, 2009). The above observations suggest that hydrated/serpentinized mantle wedge overlies all the SSE localities in the western Shikoku area. In addition, we point out here that the continental Moho beneath the Bungo Channel intersects with the subduction interface at a shallower depth than that beneath central Shikoku, resulting in a wedge of relatively cold mantle being thrust out toward the trench axis (Ueno *et al.*, 2008) (Fig. 5(c)). We suggest that this depth difference is a key to help explain the location of the long-term SSE.

The Philippine Sea plate subducting beneath southwest Japan shows considerable

variation in age (15-25 Ma) (Okino *et al.*, 1999). The age variations are symmetrically distributed around a paleo spreading axis, which is roughly perpendicular to the trench of the Nankai subduction zone. 3-D thermal modeling by Yoshioka and Murakami (2007) incorporates both the age variation within the PSP and a change in the plate motion in the Pliocene and shows that subduction of older oceanic lithosphere beneath western Shikoku is associated with significantly colder subduction than in central Shikoku (Fig. 6). These differences in temperature have important implications for the petrological nature of the mantle wedge and in turn for the distribution of long-term SSEs.

4. Slow slip behaviour controlled by the petrology of hanging wall serpentinites

Using the published thermal models, knowledge of the depth of the Moho and our petrological model of the mantle beneath Shikoku, we can estimate the temperature and pressure along the subduction boundary, and from this information estimate the petrology of the hangingwall mantle and compare it to the domains where ETS occurs （Figure 6). The calculated subduction geotherm for western Shikoku (section A in Figure 5(b)) intersects the reaction curve dividing stability fields of the Atg + Brc assemblage and the Atg + Ol assemblage at a pressure of 1.1 GPa or a depth of about 40 km (assuming a density of 2.9 g/cm^3) (Fig. 6). This depth is well below the continental Moho in the same area which lies at 25-30km (Ueno *et al.*, 2008) (Fig. 5(c)). In central Shikoku (the section B in Figure 5(b)), a warmer geotherm intersects with this reaction curve at a depth around continental Moho (Fig. 6).

The two thermal profiles for central and western Shikoku show a clear difference in the predicted mantle composition. In western Shikoku there is a 12 km layer of Atg + Brc serpentinite immediately below the Moho. At greater depths this transforms into a domain of Atg + Ol serpentinite. In contrast, in central Shikoku a warmer profile and slightly deeper Moho means that there is no brucite-antigorite region and the stable serpentinite assemblage from the moho down is Atg + Ol. The predicted difference in

mineralogy of the two sections shows a close correlation with the recorded differences in types of slow slip. Long-term slow slip recorded in western Shikoku occurs in the brucite-bearing region. Short-term slow slip is recorded in both sections. In central Shikoku this occurs in the region close to the Moho including antigorite-olivine serpentinite. In western Shikoku short-term SSE occurs within the mantle at the boundary between the Atg + Brc and Atg + Ol domains.

The correlation between the petrological analysis and geophysical observations in the Shikoku area can be extrapolated to the Tokai area in southwest Japan where one event of long-term SSE is reported (Ozawa *et al.*, 2002). This area is also likely to be underlain by a cold mantle wedge with Atg + Brc due to subduction of relatively old oceanic lithosphere (21-23 Ma) (Okino *et al.*, 1999)—although subduction of the paleo-Zenisu ridge makes the structure more complex (Kodaira *et al.*, 2004; Kato *et al.*, 2010). Our analysis suggests that the warmer Cascadia subduction zone (Peacock, 2009) should have serpentinized mantle with a mineral assemblage of Atg + Ol (Fig. 6). ETS in the Cascadia subduction zone are focused around the tip of the mantle wedge (Audet *et al.*, 2010; Schmidt and Gao, 2010) (Fig. 6) and their recurrence intervals are relatively short (5-15 months) (Dragert et al., 2001; Rogers and Dragert, 2003; Schmidt and Gao, 2010) similar to the short-term ETSs in southwest Japan.

The close spatial relationship between the ETS localities and the two types of antigorite serpentinites suggests the two are linked. This raises the question of the mechanism by which the mineralogy of serpentinite controls the different types of slow slip behaviour. The presence of brucite in fault rocks along the subduction zone will reduce the frictional strength of shallower slab-mantle boundary because the frictional coefficient of brucite under wet conditions (<0.3) (Moore and Lockner, 2007) is significantly lower than that of olivine and antigorite (about 0.6) (Moore and Lockner, 1997; Hirauchi *et al.*, 2013). However, this is inconsistent with geophysical observations that the long-term SSEs with the longer recurrence intervals—and hence also larger associated shear stresses—take place in the shallower brucite-bearing part of the mantle. This indicates that the lubricant nature of brucite cannot be directly correlated with the strength of the
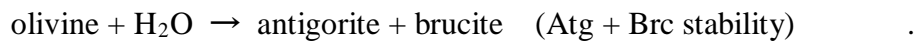
slow slip localities. Aqueous fluids from subducting slabs are likely to have high SiO_2 contents (close to quartz saturation) that may make antigorite or talc more stable at subduction boundaries rather than brucite (Peacock, 1987; Manning, 1995; Peacock and Hyndman, 1999; Frost and Beard, 2007; Hirauchi *et al.*, 2013). However, our observation of natural Atg + Brc serpentinite indicates that it can develop in mantle wedge with low SiO_2 activities probably just behind a subduction interface. Therefore, it is important to consider indirect effects of brucite-bearing mantle wedge on the state of the underlying fault plane.

Pore fluid reducing effective normal stress on fault planes is considered a key factor for the slip strengths of ETSs (Schwartz and Rokosky, 2007; Shelly *et al.*, 2007; Ide, 2010; Obara, 2011). Longer recurrence intervals and larger moment releases of long-term SSEs (Hirose and Obara, 2006) suggest larger normal stresses on the slip planes compared to those of short-term SSEs. Model calculations show effective normal stresses of 7 MPa for long-term SSEs and 1 MPa for short-term SSEs can successfully reproduce the two time-scales of recurrence observed in southwest Japan (Matsuzawa *et al.*, 2010). This result suggests extremely high pore fluid pressures for short-term SSEs and lower values for long-term SSEs.

Mantle wedge behind the fault plane may contribute to reducing the pore fluid pressure because it absorbs a significant amount of water during serpentinization. Importantly, the major serpentinization reactions consuming olivine in the Atg + Ol field is different from that in the Atg + Brc field. These can be schematically expressed as follows:

$$\text{olivine} + H_2O + SiO_2 \ \rightarrow \ \text{antigorite} \quad \text{(Atg + Ol stability)} \qquad (1)$$
and
$$\text{olivine} + H_2O \ \rightarrow \ \text{antigorite} + \text{brucite} \quad \text{(Atg + Brc stability)} \qquad .$$
$$(2)$$

Reaction (1) indicates that the extent of serpentinization in the Atg + Ol stability field depends on the amount of SiO_2 provided by an aqueous fluid; in other words, most of

the fluid is not involved in the serpentinzation reaction but remains in interstitial pore space. For example, making reasonable assumptions about quartz solubility (Gerya *et al.*, 2005) and an antigorite formula with *m*=17, reaction (1) at 500 °C and 1 GPa consumes only 1.3 mol % of the water that carries the SiO_2 required for the reaction. The limited amount of antigorite in the natural Atg + Ol serpentinite of the Higashi-akaishi ultramafic body (10-70 modal%) is consistent with this reaction. In contrast, the serpentinization reaction (2) in the Atg + Brc stability proceeds by consuming all the available water. Thus, the stability of brucite in the mantle wedge enhances its water absorbing ability. As a result, it can effectively reduce pore pressures in the surrounding region.

In conclusion, for uniform fluid supply from the subducting oceanic slab to the overlying mantle wedge, the depth-dependent change of the major serpentinization reaction will lead to a significant depth-dependent differences in pore pressure along the subduction zone boundary (Atg + Ol stability >> Atg + Brc stability). This model successfully explains the observation that the relatively strong slip planes for long-term SSEs are located in the Atg + Brc stability field and the cause of extremely high pore pressure for short-term ETSs in the Atg + Ol stability. In the Nankai subduction zone, the presence of a relatively thin serpentinized layer (or minor serpentinization) is inferred from detailed S-wave splitting analyses and receiver function analyses (Saiga *et al.*, 2013; Shibutani *et al.*, 2009). This implies that serpentinization is incomplete and the mantle wedge has the potential to cause the reaction-driven heterogeneity in pore fluid pressure. However, this mechanism may be less effective in long-lived subduction zones with highly serpentinized mantle wedge such as Cascadia (Bostock *et al.*, 2002).

We observed shear zones oblique to main foliation are dominant in the natural Atg + Brc serpentinite (i.e., S-C mylonite) (Fig. 2 and Fig. 3). This indicates that formation of soft brucite in interstitial space of platy antigorite provides a rheological heterogeneity required for localization of shear strain (Lister and Snoke, 1984). Concentration of brucite in shear zones is also observed in experimentally deformed serpentinite gouges (Moore and Lockner, 2007). These serpentinized shear zones form an anastomosing

network of interconnected spaced foliation domains that can act as pathways for fluid leading to high bulk permeability. The development of such structures in mantle wedge enhances fluid flux normal to the subduction boundary and, consequently, the flux of fluid from the boundary. Therefore, the shear structures due to the presence of soft brucite may also contribute to reduce the pore pressures in the slip planes of the long-term SSEs.

Uncertainties in geophysical, petrological and numerical estimations have been reduced by recent studies but are still significant. Vertical resolution of 3-D receiver function analyses is less than 2 km (Shiomi *et al.*, 2008; Ueno *et al.*, 2008). However, the inferred thickness of oceanic crust varies from several to 10 km (Kodaira *et al.*, 2002; Ueno *et al.*, 2008). These uncertainty and variation in the geometry of lithological structures directly affect the model calculation for the locations of the SSEs although the relative positions of inferred localities of long-term and short-term SSEs are unaffected. The incorporation of Al_2O_3 in antigorite is likely to shift the net-transfer reaction defining the boundary between the two types of antigorite serpentinite by about 10℃. The temperature shift for the reaction makes the estimated localities along the subduction boundaries about 8 km deeper (Fig. 6). If we also consider that there is some compositional variation in the mantle wedge, then it is most likely that there will be a gradual change in slow slip behaviour along a subduction boundary. Recent high resolution analyses for ETS behaviour show that typical ETS parameters are spatially variable in southwest Japan (Ide, 2010; Obara *et al.*, 2011). It should also be pointed out that thermodynamic properties for an Mg-Fe solid solution of brucite are not well constrained (e.g., Klein *et al.*, 2009), and Fe-Mg partitioning between antigorite, brucite and magnetite formed during sepentinization are not well understood. In order to discuss the relationship between serpentinization reactions and the 3D distributions of ETS in more detail, all these points require closer study.

5. Conclusions

Observations of natural serpentinite in the Sanbagawa belt and examination of a MHS phase diagram for mantle wedge compositions suggest that two types of antigorite

serpentinite—Atg + Brc serpentinite and Atg + Ol serpentinite—develop in the mantle wedge adjacent to subduction boundaries. These serpentinites are markedly different in terms of reactivity, fluid absorption and shear zone formation. The formation of Atg + Brc serpentinite absorbs large amounts of H_2O and can effectively reduce pore fluid pressure in the underlying shear zone whereas SiO_2-controlled serpentinization in Atg + Ol serpentinite will be associated with large amounts of residual fluid that helps to elevate pore fluid pressures in the vicinity.

The spatial distributions of ETSs in the Shikoku area, southwest Japan, are compared with inferred mineral assemblages in the adjacent mantle wedge, based on 3D thermal modeling and detailed observations of seismic structures. The results shows that a transition in the stable mineral assemblage from Atg + Brc to Atg + Ol with increasing depth can be correlated with the change in slip behaviour from long-term SSEs to short-term ETSs. Although there are significant uncertainties involved in the quantitative estimates, the close spatial relationships implies that metamorphic reactions in hydrated mantle may be a primary control on the slip behaviour of the subduction boundary: Atg + Ol serpentinite is responsible for extremely elevated fluid pressures in the slip planes of short-term ETSs and Atg + Brc serpentinite causes a reduction of the effective normal stresses on slip planes associated with long-term SSEs.

In general, fluid pressures on subduction boundaries are considered to fluctuate in interactive fluid systems involving influx from oceanic plate, residence and accumulation in fault planes and out flux to the mantle wedge. Based on field observations of serpentinite and geophysical data in SW Japan, we suggest that petrological controls of mantle wedge are a significant control on the type of ETS that develops. Further quantitative investigations of serpentinzation reactions and the associated structural development are important topics for constructing more accurate 3-D models for strain evolution along plate boundaries.

Acknowledgements

References

Ando, M. (1975) Source mechanisms and tectonic significance of historical earthquakes along the Nankai trough, Japan. *Tectonophys.*, **27**, 119-140.

Aoya, M., Mizukami, T. and Endo, S. (2013a) Geology of Niihama district. Chapter 3, Sanbagawa metamorphic complex. Quadrangle Series, 1:50,000, Geological Survey of Japan, AIST. p. 13-105.

Aoya, M., Endo, S., Mizukami, T. and Wallis, S. R. (2013b) Paleo-mantle wedge preserved in the Sambagawa high-pressure metamorphic belt and the thickness of forearc continental crust. *Geology*, **41**, 451-454.

Arai, S. (1994) Compositional variation of olivine-chromian spinel in Mg-rich magmas as a guide to their residual spinel peridotite. *J. Volcano. Geotherm. Res.*, **59**, 279-293.

Arai, S., Hirai, H. and Uto, K. (2000) Mantle peridotite xenoliths from the Southwest Japan arc and a model for the sub-arc upper mantle structure and composition of the Western Pacific rim. *Jour. Mineral. Petrol. Sci.*, **95**, 9-23.

Arai, S. and Ishimaru, S. (2008) Insights into petrological characteristics of the lithosphere of mantle wedge beneath arcs through peridotite xenoliths: A review. *J. Petrol.*, **49**, 665-695.

Audet, P., Bostock, M. G., Boyarko, D. C. and Brudzinski, M. R. (2010) Slab morphology in the Cascadia fore arc and its relation to episodic tremor and slip. *J. Geophys. Res.*, **115**, B00A16, doi10.1029/2008JB006053.

Bostock, M. G., Hyndman, R. D., Rondenay, S. and Peacock, S. M. (2002) An inverted continental Moho and serpentinization of the forearc mantle. *Nature*, **417**, 536-538.

Bromiley, G. D. and Pawley, A. R. (2003) The stability of antigorite in the system MgO-SiO$_2$-H$_2$O (MSH) and MgO-Al$_2$O$_3$-SiO$_2$-H$_2$O (MASH): The effects of Al^{3+} substitution on high-pressure stability. *Am. Mineral.*, **88**, 99-108.

Ide, S. (2010) Striations, duration, migration and tidal response in deep tremor. *Nature*, **466**, 356-360.

Christensen, N. I. (2004) Serpentinites, peridotites, and seismology. *Inter. Geol. Rev.*, **46**, 795-816.

Dragert, H., Wang, K. and James, T. S. (2001) A silent slip event on the deeper Cascadia subduction interface. *Science*, **292**, 1525-1528.

Enami, M., Wallis, S. R. and Banno, Y. (1994) Paragenesis of sodic pyroxene-bearing quartz schists: Implications for the P-T history of the Sanbagawa belt. *Contrib. Mineral. Petrol.*, **116**, 182-198.

Enami, M., Mizukami, T. and Yokoyama, K. (2004) Metamorphic evolution of garnet-bearing ultramafic rocks from the Gongen area, Sanbagawa belt, Japan. *J. Metamorph. Geol.*, **22**, 1-15.

Endo, S. (2010) Pressure-temperature history of titanite-bearing eclogite from the Western Iratsu body, Sanbagawa Metamorphic Belt, Japan. *Island Arc*, **19**, 313-335.

Evans, B. W. (2004) The serpentine multisystem revisited: Chrysotile is metastable. *Inter. Geol. Rev.*, **46**, 479-506.

Frost, B. R. and Beard, J. S. (2007) On silica activity and serpentinization. *J. Petrol.*, **48**, 1351-1368.

Gerya, T. V., Maresch, W. V., Burchard, M., Zakhartchouk, V., Doltsinis, N. L. and Fockenberg, T. (2005) Thermodynamic modeling of solubility and speciation of silica in H_2O-SiO_2 fluid up to 1300 °C and 20 kbar based on the chain reaction formalism. *Eur. J. Mineral.*, **17**, 269-283.

Hattori, K., Wallis, S., Enami, M. and Mizukami, T. (2010) Subduction of mantle wedge peridotites: Evidence from the Higashi-akaishi ultramafic body in the Sanbagawa metamorphic belt. *Island Arc*, **19**, 192-207.

Hellebrand, E., Snow, J. E., Dick, H. J. B. and Hofmann, A. W. (2001) Coupled major and trace elements as indicators of the extent of melting in mid-ocean-ridge peridotites. *Nature*, **410**, 677-681.

Higashino, T. (1990) The higher-grade metamorphic zonation of the Sambagawa metamorphic belt in central Shikoku, Japan. *J. Metamorph. Geol.*, **8**, 413-423.

Hiramatsu, Y., Watanabe, T. and Obara, K. (2008) Deep low frequency tremors as a proxy for slip monitoring at plate interface. *Geophys. Res. Let.*, **35**, L13304.

Hirauchi, K.-I., Sabine, A. M., den Hartog, S. A. M., Spiers, C. J. (2013) Weakening of the slab-mantle wedge interface induced by metasomatic growth of talc. *Geology*, **41**, 75-78.

Hirose, H. and Obara, K. (2006) Repeating short- and long-term slow slip events with deep tremor activity around the Bungo channel region, southwest Japan. *Earth Planets Space*, **57**, 961-972.

Hostetler, P. B., Coleman, R. G., Mumpton, F. A. and Evans, B. W. (1966) Brucite in alpine serpentinites. *Am. Min.*, **51**, 75-98.

Hyndman, R. D. and Peacock, S. M. (2003) Serpentinization of the forearc mantle.

Earth Planet. Sci. Let., **212**, 417-432.

Ide, S. (2010) Striations, duration, migration and tidal response in deep tremor. *Nature*, **466**, 356-359.

Ito, T., Kojima, Y., Kodaira, S., Sato, H., Kaneda, Y., Iwasaki, T., Kurashimo, E., Tsumura, N., Fujiwara, A., Miyauchi, T., Hirata, N., Harder, S., Miller, K., Murata, A., Yamakita, S., Onishi, M., Abe, S., Sato, T. and Ikawa, T. (2009) Crustal structure of southwest Japan, revealed by the integrated seismic experiment Southwest Japan 2002. *Tectonophys.*, **472**, 124-134.

Kanamori, H. (1972) Tectonic implications of the 1944 Tonankai and the 1946 Nankaido earthquakes. *Phys. Earth Planet. Inter.*, **5**, 129-139.

Katayama, I., Terada,T., Okazaki, K. and Tanikawa, W. (2012) Episodic tremor and slow slip potentially linked to permeability contrasts at the Moho. *Nature Geoscience*, **5**, 731–734.

Kato, A., T. Iidaka, R. Ikuta, Y. Yoshida, K. Katsumata, T. Iwasaki, S. Sakai, C. Thurber, N. Tsumura, K. Yamaoka, T. Watanabe, T. Kunitomo, F. Yamazaki, M. Okubo, S. Suzuki, N. Hirata (2010) Variations of fluid pressure within the subducting oceanic crust and slow earthquakes, *Geophys. Res. Lett.*, **37**, L14310, doi:10.1029/2010GL043723

Kodaira, S., Kurashimo, E., Park, J.-O., Takahashi, N., Nakanishi, A., Miura, S., Iwasaki, T., Hirata, N., Ito, K. and Kaneda, Y. (2002) Structural factors controlling the rupture process of a megathrust earthquake at the Nankai trough seismogenic zone. *Geophys. J. Int.*, **149**, 815-835.

Kodaira, S., Iidaka, T., Kato, A., Park, J.-O., Iwasaki, T. and Kaneda, Y. (2004) High pore fluid pressure may cause silent slip in the Nankai trough. *Science*, **304**,

1295-1298.

Kouketsu, Y., Enami, M. and Mizukami, T. (2010) Omphacite-bearing metapelite from the Besshi region, Sambagawa metamorphic belt, Japan: Prograde eclogite facies metamorphism recorded in metasediment. *J. Mineral. Petrol. Sci.*, **105**, 9-19.

Kunugiza, K. (1980) Dunites and serpentinites in the Sanbagawa metamorphic belt, central Shikoku and Kii peninsula, Japan. *J. Japan. Assoc. Min. Petrol. Econ. Geol.*, **75**, 14-20.

Kunugiza, K. (1984) Metamorphism and origin of ultramafic bodies of the Sanbagawa metamorphic belt in central Shikoku. *J. Japan. Assoc. Min. Petrol. Econ. Geol.*, **79**, 20-32. (In Japanese with English abstract)

Lister, G. S. and Snoke, A. W. (1984) S-C mylonites. *J. Structural. Geol.*, **6**, 617-638.

Matsuzawa, T., Hirose, H., Shibazaki, B. and Obara, K. (2010) Modeling short- and long-term slow slip events in the seismic cycles of large subduction earthquakes. *J. Geophys. Res.*, **115**, B12301.

Manning C. E. (1995) Phase-equilibrium controls on SiO_2 metasomatism by aqueous fluid in subduction zones: Reaction at constant pressure and temperature. *Inter. Geol. Rev.*, **37**, 1074-1093.

Matsubara, M., Obara, K. and Kasahara, K. (2009) High-V_P/V_S zone accompanying non-volcanic tremors and slow-slip events beneath southwestern Japan. *Tectonophys.*, **472**, 6-17.

Mellini, M., Trommsdorff, V. and Companioni, R. (1987) Antigorite polysomatism: Behaviour during progressive metamorphism. *Contrib. Mineral. Petrol.*, **97**, 147-155.

Mizukami, T. and Wallis, S. R. (2005) Structural and petrological constraints on the tectonic evolution of the garnet-lherzolite facies Higashi-akaishi peridotite body, Sanbagawa belt, SW Japan. *Tectonics*, **24**, TC6012.

Moore, D. E. and Lockner, D. A. (1997) Strengths of serpentinite gouges at elevated temperatures. *J. Geophys. Res.*, **102**, 14787-14801.

Moore, D. E. and Lockner, D. A. (2007) Comparative deformation behavior of minerals in serpentinized ultramafic rocks: Application to the slab-mantle interface in subduction zones. *Inter. Geol. Rev.*, **49**, 401-415.

Mouri, T. and Enami, M. (2008) Areal extent of eclogite facies metamorphism in the Sanbagawa belt, Japan: New evidence from a Raman microprobe study of quartz residual pressure. *Geology*, **36**, 503-506.

Obara, K. (2002) Nonvolcanic deep tremor associated with subduction in southwest Japan. Science, 296, 1679-1681.

Obara, K. (2010) Phenomenology of deep slow earthquake family in southwest Japan: Spatiotemporal characteristics and segmentation. *J. Geophys. Res.*, **37**, L13306, doi:10.1029/2010GL043679.

Obara, K. (2011) Characteristics and interactions between non-volcanic tremor and related slow earthquakes in the Nankai subduction zone, southwest Japan. *J. Geodyn.*, **52**, 229-248.

Obara, K. and Hirose, H. (2006) Nonvolcanic deep low-frequency tremors accompanying slow slips in the southwest Japan subduction zone. *Tectonophys.*, **417**, 33-51.

Obara, K., Matsuzawa, T., Tanaka, S., Kimura, T. and Maeda, T. (2011) Migration properties of non-volcanic tremor in Shikoku, southwest Japan. *Geophys. Res. Lett.*, **38**, L09311, doi:10.1029/2011GL047110.

O'Hanley, D. S. (1996) *Serpentinites*. Oxford University Press, New York, 277pp.

Okino, K., Ohara, Y., Kasuga, S. and Kato, Y. (1999) The Philippine Sea: New survey results reveal the structure and the history of the marginal basins. *Geophys. Res. Let.*, **26**, 2287-2290.

Ozawa, S., Murakami, M., Kaidzu, M., Tada, T., Sagiya, T., Hatanaka, Y., Yarai, H. and Nishimura, T. (2002) Detection and monitoring of ongoing aseismic slip in the Tokai region, central Japan. *Science*, **298**, 1009-1012.

Padrón-Navarta, J. A., Hermann, J., Garrido, C. J., Sánchez-Vizcaíno, V. L. and Gómez-Pugnaire, M. T. (2010) An experimental investigation of antigorite dehydration in natural silica-enriched serpentinite. *Contrib. Minral. Petrol.*, **159**, 25-42.

Padrón-Navarta, J. A., Sánchez-Vizcaíno, V. L., Hermann, J., Connolly, J. A. D., Garrido, C. J., Gómez-Pugnaire, M. T. and Marchesi, C. (2013) Tschermak's substitution in antigorite and consequences for phase relations and water liberation in high-grade serpentinites. *Lithos*, **178**, 186-196.

Parkinson, I. J. and Pearce, J. A. (1998) Peridotites from the Izu-Bonin-Mariana forearc (ODP Leg 125): Evidence for mantle melting and melt-mantle interaction in a supra-subduction zone setting. *J. Petrol.*, **39**, 1577-1618.

Peacock, S. M. (1987) Serpentinization and infilteration metasomatism in the Trinity peridotite, Klamath province, northern California. *Contrib. Mineral. Petrol.*, **95**, 55-70.

Peacock , S. M. (2009) Thermal andmetamorphic environment of subduction zone episodic tremor and slip. *J. Geophys. Res.*, **114**, B00A07, doi10.1029/2008JB005978

Peacock, S. M. and Hyndman, R. D. (1999) Hydrous minerals in the mantle wedge and the maximum depth of subduction thrust earthquakes, *Geophys. Res. Let.*, **26**, 2517-2520.

Rogers, G. and Dragert, H. (2003) Episodic tremor and slip on the Cascadia subduction zone: The chatter of silent slip. *Science*, **300**, 1942-1943.

Rubinstein, J. L., La Rocca, M., Vidale, J. E., Creager, K. C. and Wech, A. G. (2008) Tidal modulation of nonvolcanic tremor. *Science*, **319**, 186-189.

Rubinstein, J. L., Vidale, J. E., Gomberg, J., Bodin, P., Creager, K. C. and Malone, S. D. (2007) Non-volcanic tremor driven by large transient shear stress. *Nature*, **448**, 579-582.

Schmidt, D. A. and Gao, H. (2010) Source parameters and time-dependent slip distributions of slow slip events on the Cascadia subduction zon from 1998 to 2008. *J. Geophys. Res.*, **115**, B00A18, doi10.1029/2008JB006045.

Schwartz, S. Y. and Rokosky, J. M. (2007) Slow slip events and seismic tremor at circum-Pacific subduction zones. *Rev. Geophys.*, **45**, RG3004.

Sekine, S., Hirose, H. and Obara, K. (2010) Along-strike variations in short-term slow slip events in the southwest Japan subduction zone. *J. Geophys. Res.*, **115**, B00A27.

Shelly, D. R., Beroza, G. C., Ide, S. and Nakamura, S. (2006) Low-frequency earthquakes in Shikoku, Japan, and their relationship to episodic tremor and slip.

Nature, **442**, 188-191.

Shiomi, K., Matsubara, M., Ito, Y. and Obara, K. (2008) Simple relationship between seismic activity along Philippine Sea slab and geometry of oceanic Moho beneath southwest Japan. *Geophys. J. Int.*, **173**, 1018-1029.

Sibutani, T., Hirahara, K. and Ueno, T. (2009) Receiver function analyses for estimating seismic velocity discontinuity structure. *J. Seis. Soc. Japan. 2nd ser.*, **61**, S199-S207 (In Japanese with English abstract)

Tatsumi, Y. (2006) High-Mg andesites in the Setouchi volcanic belt, southwest Japan: Analogy to Archean magmatism and continental crust formation? *Annu. Rev. Earth Planet. Sci.*, **34**, 467-499.

Ueno, T., Shibutani, T. and Ito, K. (2008) Configuration of the continental Moho and Phlippine Sea slab in southwest Japan derived from receiver function analysis: relation to subcrustal earthquakes. *Bull. Seis. Soc. Am.*, **98**, 2416-2427.

Ulmer, P. and Trommsdorff, V. (1995) Serpentine stability to mantle depths and subduction-related magmatism. *Science*, **268**, 858-861.

Ulmer, P. and Trommsdorff, V. (1999) Phase relations of hydrous mantle subducting to 300 km. In *Mantle Petrology: Field Obervations and High Pressure Experimentation* (eds: Fei Y., Bertka, C. M. & Mysen, B. O.), 259-281.

Wicks, F. J., Whittaker, E. J. W. and Zussman, J. (1977) An idealized model for serpentine textures after olivine. *Can. Min.*, **15**, 446-458.

Wunder, B. and Schreyer, W. (1997) Antigorite: High-pressure stability in the system $MgO\text{-}SiO_2\text{-}H_2O$ (MSH). *Lithos*, **41**, 213-227.

Yoshioka, S. and Murakami, K. (2007) Temperature distribution of the upper surface of the subducted Philippine Sea Plate along the Nankai Trough, southwest Japan, from a three-dimensional subduction model: relation to large interpolate and low-frequency earthquakes. *Geophys. J. Int.*, **171**, 302-315.

Figure captions

Figure 1

(a) Geological map of the Sanbagawa metamorphic belt in central Shikoku, Japan (after Kunugiza (1984), Higashino (1990) and Aoya *et al*. (2013a)). Distributions of ultramafic bodies and major metagabbro bodies are shown in the map. Metamorphic zones are defined by mineral assemblages in pelitic schist: Oligoclase-Biotite (Olg-Bt) zone, Albite-Biotite (Ab-Bt) zone, Garnet (Grt) zone and Chlorite (Chl) zone.

(b) Geological map of the Higashi-akaishi ultramafic body. The north dipping 400 m-thick tabular unit lies on metamorphosed accretionary units consisting of basic and pelitic schists. The upper boundary is limited by a garnet amphibolite unit with petrological evidence of eclogite facies metamorphism. Antigorite-rich rocks are dominant in the marginal part of this body. The central part preserves older microstructures defined by olivine and Cpx.

(c) Geological map of the Shiraga ultramafic body. Circles indicate occurrence of brucite-bearing serpentinite. Open circles indicate samples with microtextural evidence for metamorphic olivine after antigorite and brucite. Broken lines show boundaries between the metamorphic zones.

Figure 2

Mesoscopic and microscopic structures of antigorite serpentinites in the Higashi-akaishi body. Atg = antigorite, Brc = brucite, Mgt = magnetite, Ol = olivine.

(a) Outcrop view of a layered structure in partly serpentinized dunite. Antigorite-rich layers stand out on the surface (sub-normal to the foliation) due to high resistivity of antigorite against weathering. Small displacements across the layers are associated with lizardite. Hammer head = 18 cm.

(b) Outcrop view of a sheared structure in an antigorite-rich layer. Antigorite shear zones (SZ) with spacing of several centimeters crosscut the main foliation (S) defined by parallel alignment of antigorite, showing a sinistral sense of shear.

(c) Microphotograph of a direct contact between olivine and antigorite in less

serpentinized layers. Platy crystals of antigorite have grown at olivine grain boundaries and locally intrude into olivine. Cross polarized light.

(d) Microphotograph shows an antigorite-rich shear zone (SZ) crosscutting a foliation (S) defined by a parallel orientation of platy antigorite and olivine. Antigorite in the foliation forms discrete grains among olivine whereas it occurs as bundles in the shear zone. Parallel alignment of antigorite crystals in the shear zones and foliations provides permeable fluid pathways. Cross polarized light.

(e) Close-up of the antigorite-rich shear zone (a rectangle in (d)). Brucite (yellowish colour in crossed polars) occurs as films at interspaces of platy antigorite. Minor proportion of brucite is partly due to reaction with aqueous silica to form antigorite. Magnetite between antigorite plates represents release of Fe during the reaction. Cross polarized light.

(f) Micro-Raman analyses for the minerals in the shear zone at the points A and B in (e). The spectrum for the point A shows typical O-H stretching bands of antigorite. The spectrum for the point B includes O-H bands of both brucite and antigorite. The Raman O-H peak at 3650 cm^{-1} is characteristic to $Mg(OH)_2$ brucite and a peak at 3642 cm^{-1} indicates that a significant amount of Fe is contained in the hydroxide. The Raman analyses are made for thin sections under an optical microscope (BX41, Olympus) using an Ar+ laser with a wave length of 514.5 nm (Series 543-400-A06, Melles Griot) and a spectrometer (LabRAM HR800, Horiba-Jobin Yvon) with a 1800/mm grating and a Si-based CCD detector of 1024×256 pixels.

Figure 3
Mesoscopic and microscopic structures of antigorite serpentinites in the Shiraga body. Abbreviations are same as in Figure 4.

(a) Outcrop view of sheared antigorite serpentinite with brecciated blocks showing a dextral displacement along their contact. Hammer head = 18 cm.

(b) Microphotograph of a 'mesh-rim'-like texture consisting of antigorite and metamorphic olivine in a massive block. Platy crystals of antigorite align normal to edges of mesh cells and olivine rims the mesh cells. No talc was found. Cross polarized light.

(c) Microphotograph of ductile S-C structure in sheared antigorite serpentinite. Brucite with a high refractive index forms layers (veins) parallel to S planes. Darker parts of the layers consist of magnetite and antigorite in addition to brucite, indicating silica metasomatism along the layers. Magnetite is characteristically formed along C planes. Plane polarized light.

(d) Close up of a rectangle in (c). Brucite layers are sub-parallel to S defined by an alignment of platy antigorite. Cross polarized light.

(e) Microphotograph showing a concentration of brucite in a shear plane cross-cutting porphyroblastic olivine. Brucite shows undulose extinction. Cross polarized light.

(f) Micro-Raman analyses for the minerals in the shear zone at the points C and D in (d). The spectrum for the point C shows O-H stretching bands of antigorite. The spectrum for the point D includes O-H bands of both brucite and antigorite.

Figure 4

P-T evolutions proposed for the Higashi-akaishi ultramafic body (Enami *et al.*, 2004; Mizukami and Wallis, 2005) and the Shiraga ultramafic body (Enami *et al.*, 1994) and selected reaction curves for hydrous peridotite. Atg = antigorite; Brc = brucite; Di = diopside, En = enstatite; Fo = forsterite; Tlc = talc; Tr = tremolite, W = water.

Figure 5

Seismic structures and distributions of ETS in southwest Japan. (a) Epicenters of tremors (low-frequency earthquakes, strictly) (black circles) and localities of SSEs (long-term: blue line; short-term: red line) are after Obara (2002), Hirose and Obara (2006) and Sekine *et al.* (2010). Long-term SSEs in Tokai and Bungo Channel areas overlaps the tremor sources. Light blue broken lines enclose the source regions for the Nankai, Tonankai and Tokai mega-thrust earthquakes. (b) V_P/V_S tomography and distribution of tremors (black circles) in western Shikoku area at the depth of 30 km (Matsubara *et al.*, 2009). The estimated slip planes for the Bungo Channel long-term SSE overlaps a high V_P/V_S zone. No association of low frequency tremor at the shallower parts is characteristic to long-term SSEs. (c) Seismic cross-sections of central

Shikoku (line A in (b), top) and western Shikoku (line B, bottom) including results of V_P/V_S tomography (Matsubara *et al.*, 2009) and receiver function analyses for continental Moho (Ueno *et al.*, 2008) and subduction boundaries (Shiomi *et al.*, 2008). SSE localites are also projected to the sections; S-SSE = short-term SSE and L-SSE = long-term SSE.

Figure 6

MSH phase diagram and ETS distributions along subduction boundaries. Reaction curves for the MSH system refer to Ulmer and Trommsdorff (1999), Bromiley and Pawley (2003) and Evans (2004). Stability of mineral assemblages in harzburgite (Ol>70%): Liz + Atg (purple), Atg + Brc (green), Atg + Ol (blue) and Ol + Opx/Tlc (orange). The phase diagram predicts the variations of mantle minerals along subduction boundaries in southwest Japan (A and B in Figure 5(b)) (Yoshioka and Murakami, 2007) and northern Cascadia (Peacock, 2009). Abbreviations: Atg = antigorite; Brc = brucite; En = enstatite; Fo = forsterite; Liz = lizardite; Ol = olivine; Opx = orthopyroxene; Tlc = talc; W = water. The right columns show estimated hanging wall materials along the subduction boundaries and ETS localities. ETS data: SW Japan (Hirose and Obara, 2006); Cascadia (Audet *et al.*, 2010; Schmidt and Gao, 2010). The results indicate that the physical properties of the plate interfaces are highly variable depending on thicknesses of continental crusts and thermal conditions of subduction zones. In western Shikoku (B), the depth range of the slip plane for long-term SSE (blue bar) overlaps the Atg + Brc stability whereas deep tremors (stars) and short-term SSEs (indicated in red bars) mostly take place within the Atg + Ol stability.
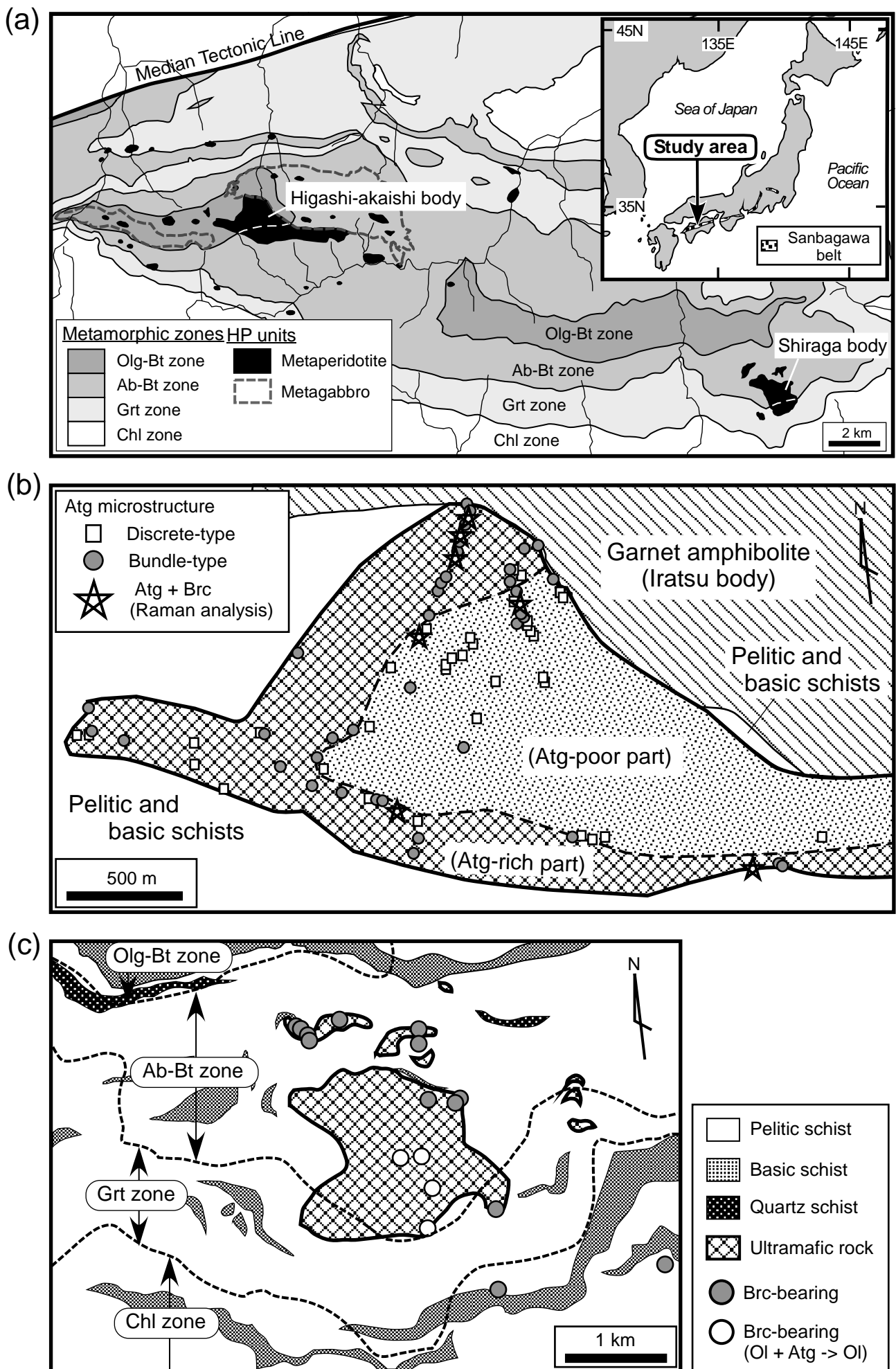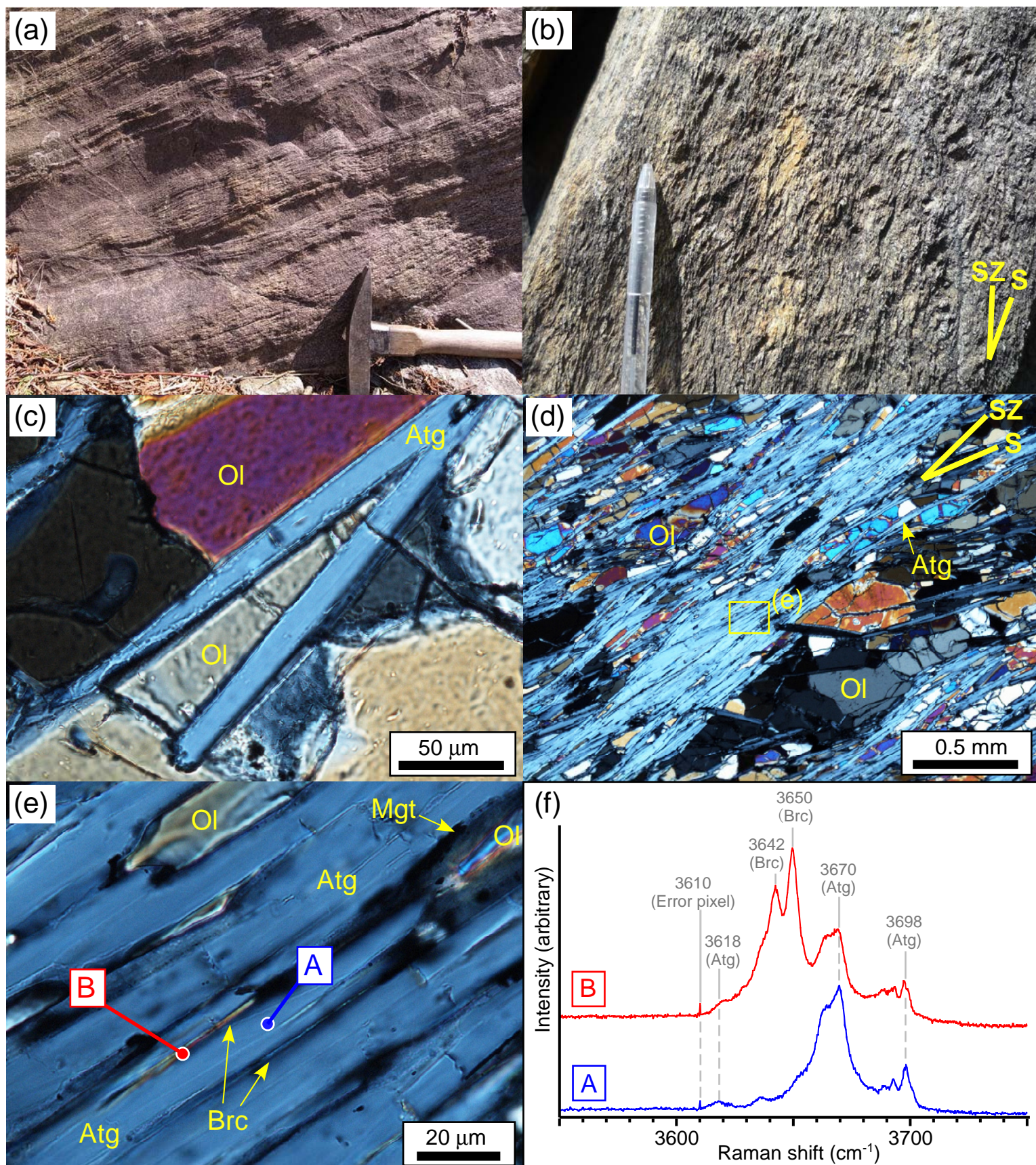
Figure 1 (Mizukami et al., EPSL)
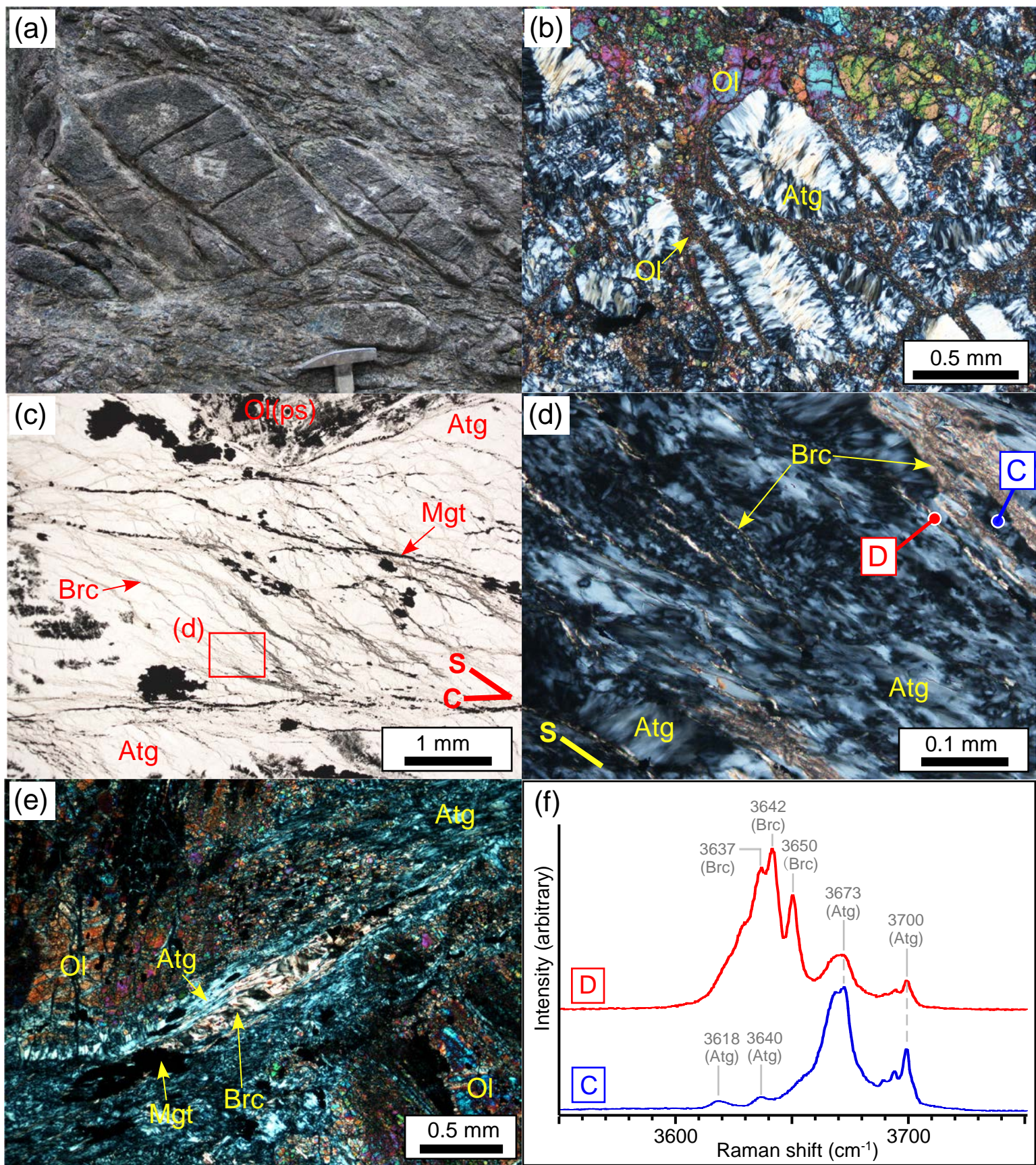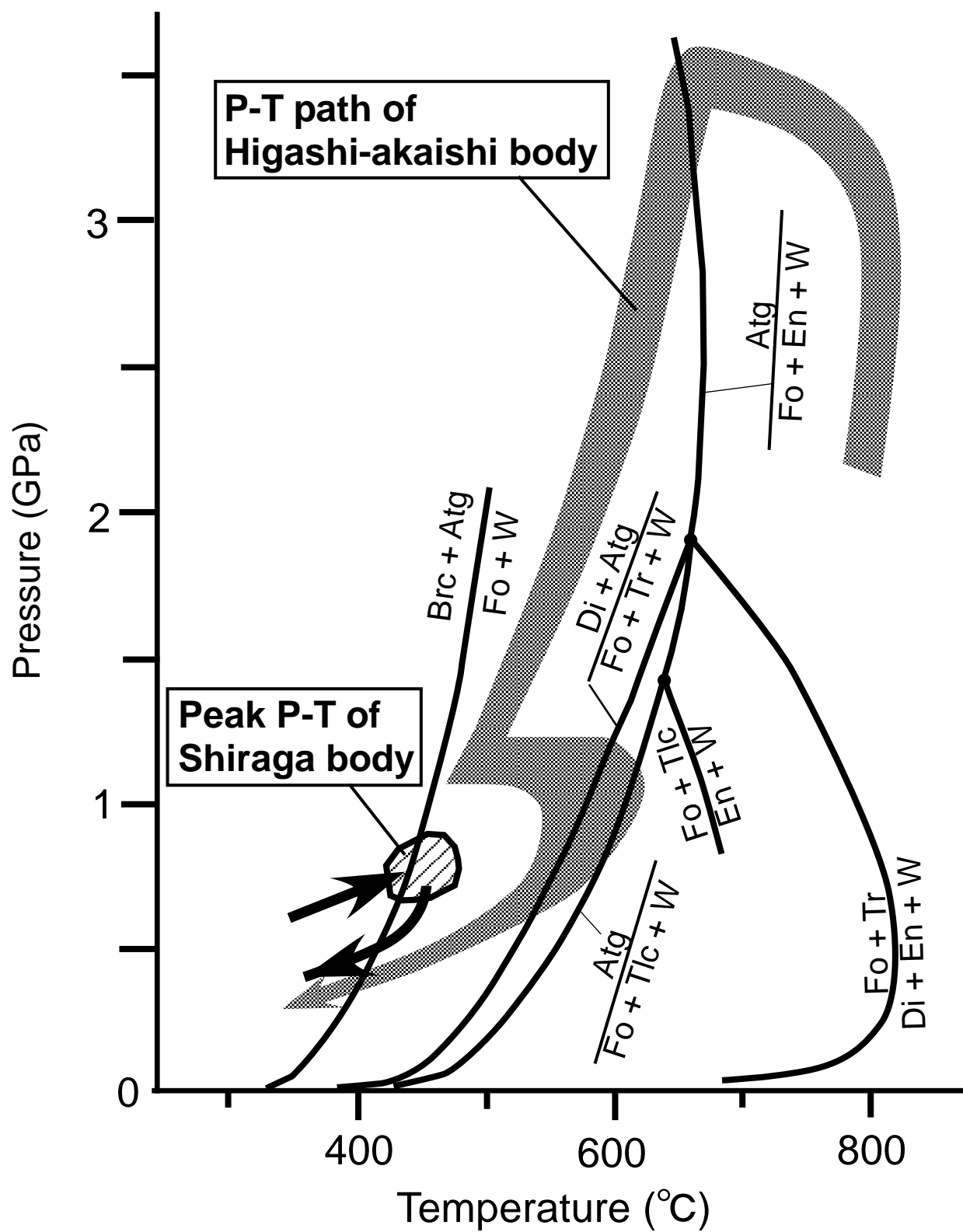
Figure 2 (Mizukami et al., EPSL)

Figure 3 (Mizukami et al., EPSL)

(a)

Tokai

Bungo
Channel

Nankai

Tonankai

Tokai

Nankai Trough

100 km

(b)

(Depth = 30km)

70km 60km 50km

40km

30km

20km

2003/08
−2004/04

2009/08
−2010/02

2010/02
−2010/10

1997/03
−1997/12
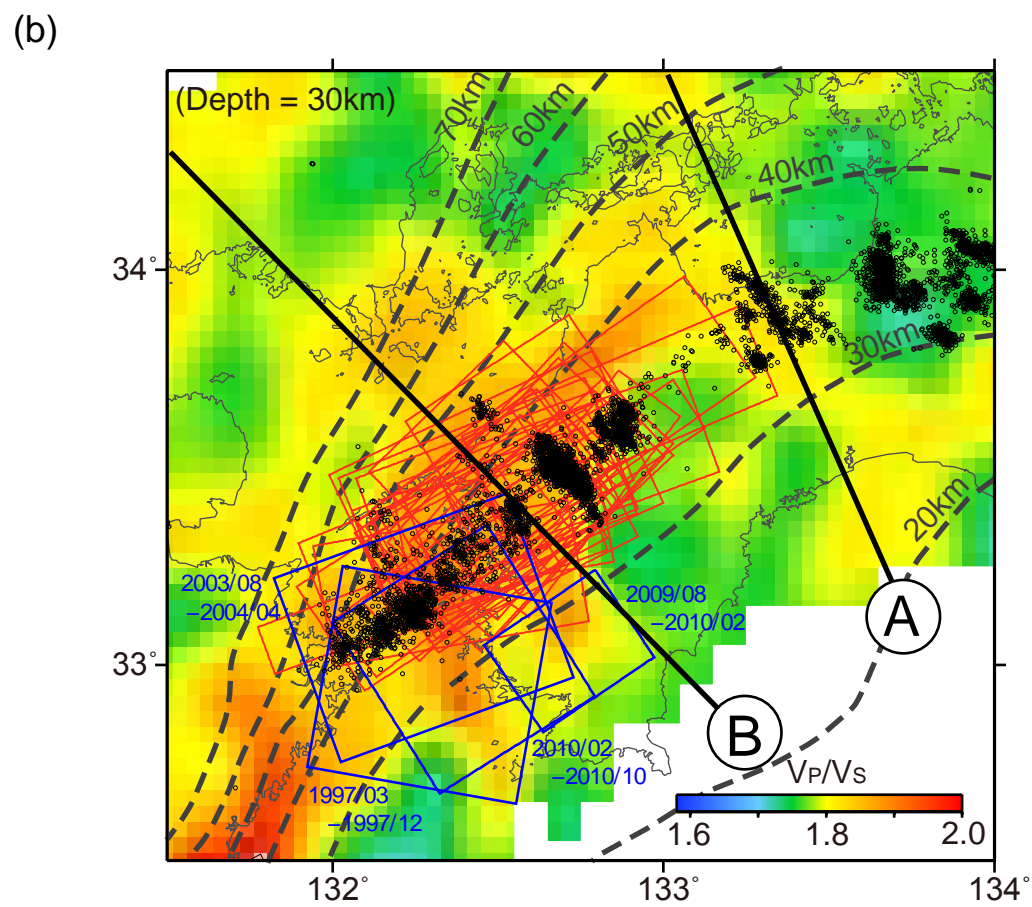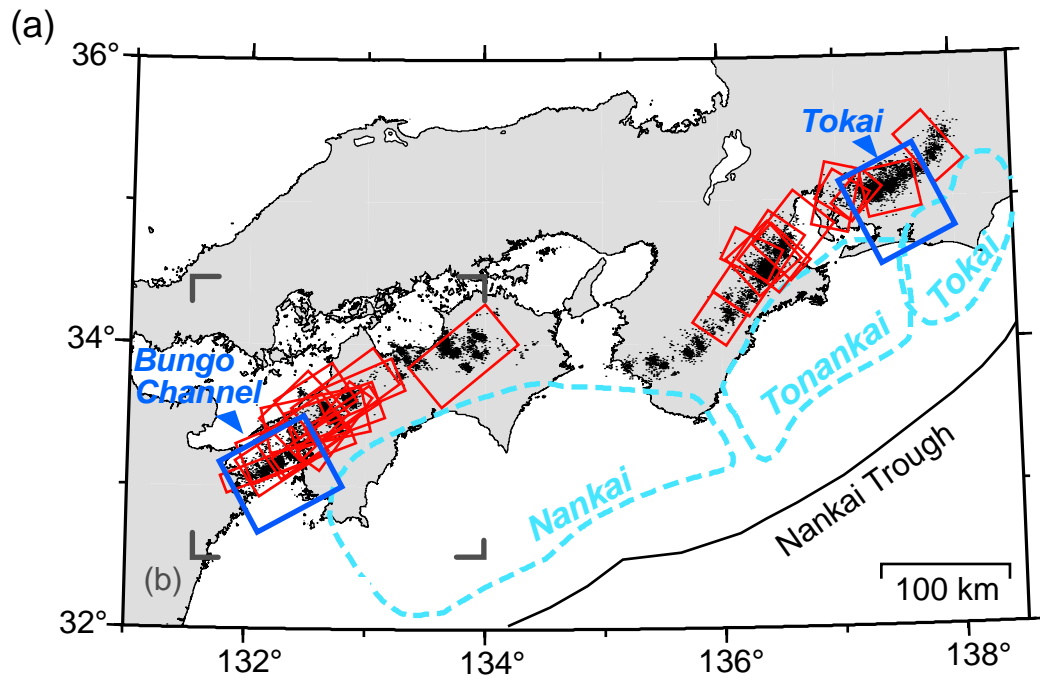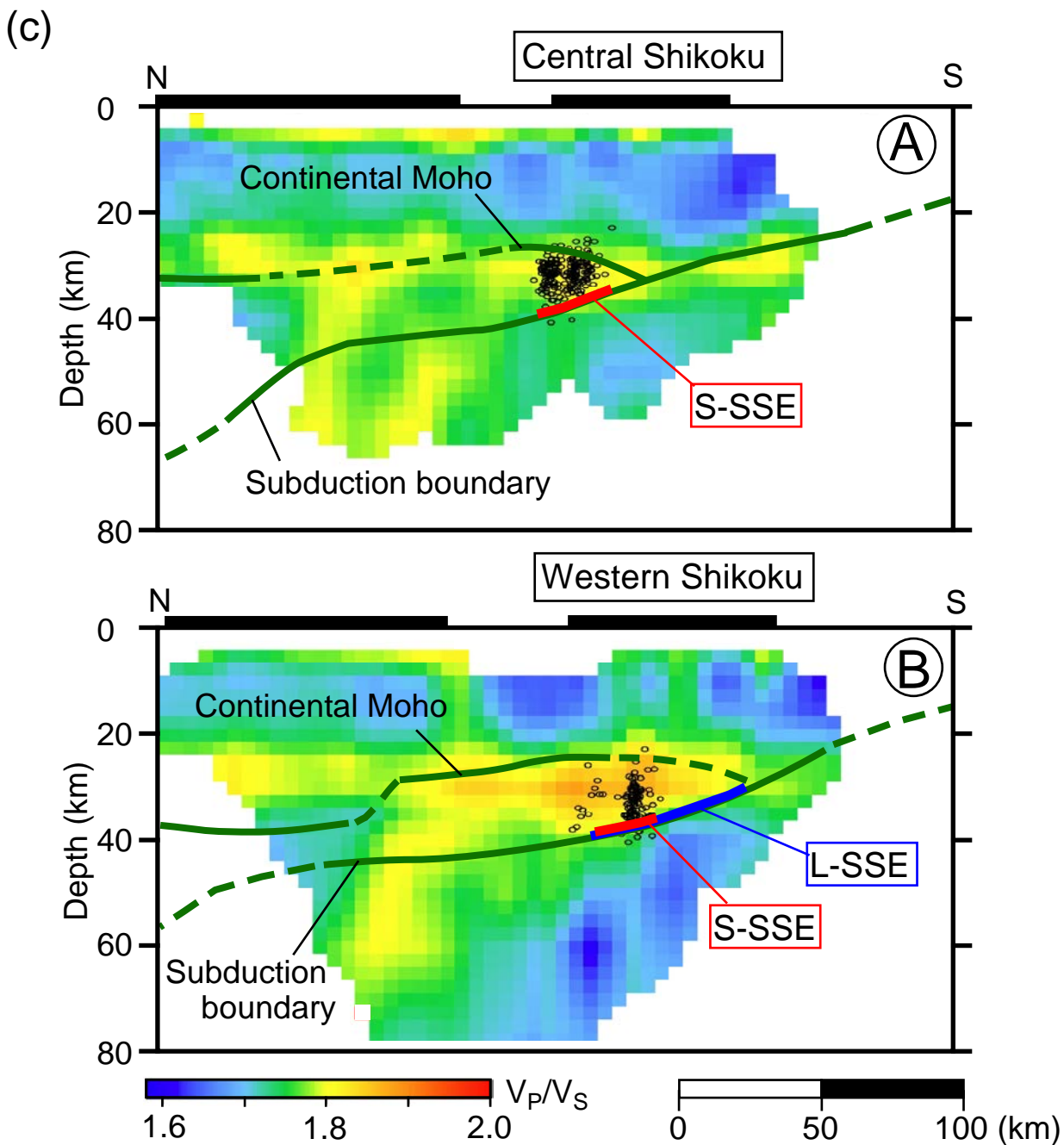
A

B

V_P/V_S

1.6   1.8   2.0

Figure 5 (a) and (b) (Mizukami et al., EPSL)

Figure 5 (c) (Mizukami et al., EPSL)

Figure 6 (Mizukami et al., EPSL)